Optimization of photoluminescence of Eu^{3+} doped YVO$_4$ nanoparticles by green microwave synthesis

Houssem Eddine Sekrafi [a,b,*], Eya Hergli [a,b], Stanislav Ferdov [a,b], André Mota [c], Joni Lopes [c], Paulo J.G. Coutinho [a,b], Luis Rebouta [a,b]

[a] *Physics Centre of Minho and Porto Universities (CF-UM-UP), University of Minho, 4710-057, Braga, Portugal*
[b] *Laboratory of Physics for Materials and Emergent Technologies, LaPMET, University of Minho, 4710-057, Braga, Portugal*
[c] *Sonae Arauco Portugal, SA, Lugar Do Espido - Via Norte, Apartado 1129, 4470-177, Maia, Porto, Portugal*

HIGHLIGHTS

- Red YVO$_4$:Eu^{3+} phosphor investigated via green microwave synthesis.
- Increasing the concentration of Eu dopant reduces the degree of agglomeration.
- An aqueous YVO$_4$:Eu^{3+} colloidal solution showed a stable zeta potential of 34 mV.
- Only water as a solvent, pH = 6, yielded samples with the highest emission intensity.

GRAPHICAL ABSTRACT
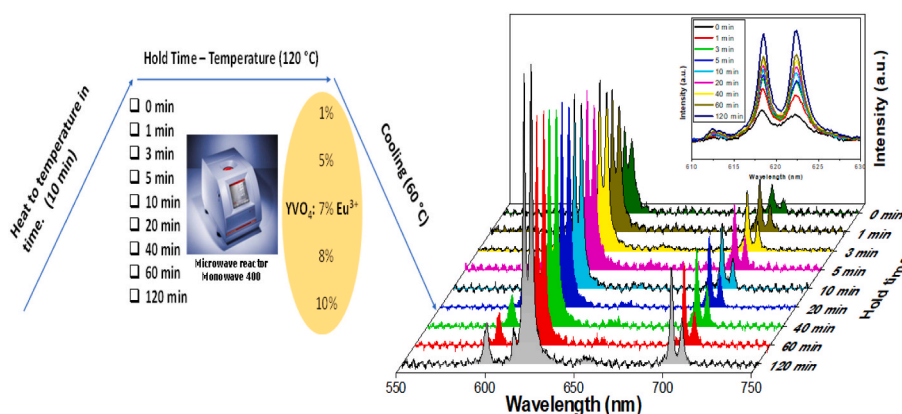
ARTICLE INFO

ABSTRACT

A detailed investigation of the europium-doped yttrium orthovanadate (YVO$_4$:Eu^{3+}) phosphorus prepared by fast and facile microwave synthesis was undertaken. The phase purity, morphology, particle distribution analysis, and photoluminescence were all thoroughly examined. The photoluminescence (PL) properties of the as-synthesized YVO$_4$:Eu^{3+} nanostructures depend greatly on the synthesis parameters. The PL intensity of the nanomaterials increased when the Eu concentration, holding time, and amount of water used in the prepared phosphors were adjusted. The optimal europium doping concentration was 7 mol% for temperature holding times of 60 min, and 5 ml of water was used as the solvent. The emission intensity of Eu^{3+}-doped YVO$_4$ phosphors can be rationally modified by simply changing the pH of the solution or by employing different solvents. The phosphors studied were produced as nanoparticles with a very intense emission spectrum, making them good candidates for fluorescent lamps and light-emitting diodes (LEDs).
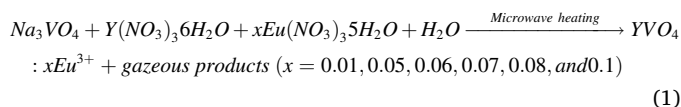
---

1. Introduction

Because of their significant spectrum of applications in industry, technology, and fundamental science, nanostructured phosphors are attracting the interest of researchers. As a result, scientists are working diligently to develop novel methods to produce rare-earth-doped phosphors with improved luminescence properties [1–5]. The controlled and environmentally friendly synthesis of inorganic materials with well-defined characteristics like particle size, optical performance, crystal structure, and others is an important step for their sustainable large-scale applications. Lanthanide ion-activated phosphors have received a lot of attention among luminescence materials because of their wide range of emission colors and excellent luminescent performance [6]. In particular, rare-earth element doped yttrium orthovanadate (YVO_4) phosphors are widely used in medical and biomedical applications, including fluorescence resonance energy transfer (FRET) diagnostics, bio-labeling, and phototherapy, industrial sensors, and solar cells owing to their excellent optical, electrical, and magnetic properties [7–10]. Along with its appropriate crystal structure and excellent chemical stability [11], YVO_4 has shown to be an effective host lattice for rare earth ions to make phosphors emitting a variety of colors [12]. Especially, YVO_4:Eu^{3+} nanocrystals have optical characteristics and minimal cytotoxicity, making them appealing for biological applications, and YVO_4:Eu^{3+} nanocrystals have already been employed to detect biomolecules [13]. All of these features motivated the researchers to develop economical and suitable methods for producing extremely stable and scalable phosphors [14–16]. In recent decades, extensive effort has been expended to synthesize inorganic phosphors with fine particle size, controllable morphologies, and high luminescence efficiency [17,18]. These functional materials doped with rare earth ions have been synthesized by the conventional solid-state method [19,20]; it is indeed simple but has various limitations, such as high energy consumption and agglomeration of particles. On the basis of wet chemistry approaches, such as sol-gel procedure [21], modified combustion synthesis [22], co-precipitation reaction [23], ultrasonic method [24], and hydrothermal method [25] were found to be more effective than the classical method in producing single-phase and well-crystalline YVO_4. Considering the phosphor synthesis strategy, we can note that the hydrothermal method is one of the most valuable methods for the production of YVO_4 doped with phosphors because it can produce particles with excellent crystallinity, narrow size distribution, and high purity under mild reaction conditions without milling or extra annealing temperature [26].

There are a variety of protocols used to produce luminescent nanoparticles of YVO_4 by microwave processing [27–30]. Among them, a considerable amount of research is focused on exploring crystal growth and luminescence properties in connection with the morphology of Eu^{3+}-doped YVO_4 [31,32]. However, the crystallization is at relatively high temperatures (between 180 °C and 300 °C) and for long periods of time (2 h, 6 h, 12 h, and 24 h). Additionally, these methods often involve the use of various additives, such as ethanol, polyethylene glycol, and polyvinylpyrrolidone, among others – all of which we intentionally avoid in our approach. In this context the purpose of this study is to demonstrate environmentally friendly and energetically efficient microwave synthesis of YVO_4:Eu^{3+} nanoparticles by using decreased temperature and short synthesis time. In addition, the effects of microwave heating for different times, amounts of water, pH value of solution and Eu concentrations on photoluminescent properties were studied to determine the optimal emission spectra.

2. Materials and methods

We have used, precursors purchased from Sigma-Aldrich (St. Louis, MO, USA), sodium othovanadate Na_3VO_4 (99.98% trace metals basis), yttrium nitrate hexahydrate $Y(NO_3)_3 \bullet 6H_2O$ (purity of 99.9%) and europium (III) nitrate pentahydrate $Eu(NO_3)_3 \bullet 5H_2O$ (purity of 99.9%)

in the desired proportion. They were mixed according to the following reaction [33]:

$$Na_3VO_4 + Y(NO_3)_3 6H_2O + xEu(NO_3)_3 5H_2O + H_2O \xrightarrow{Microwave\ heating} YVO_4$$
$$: xEu^{3+} + gazeous\ products\ (x = 0.01, 0.05, 0.06, 0.07, 0.08, and 0.1)$$

(1)

1 mmol of Na_3VO_4 was dissolved in 4 ml of distilled water. Subsequently, 1 mmol $Y(NO_3)_3 \bullet 6H_2O$ was dissolved in 0.5 ml of distilled water. Following that, the desired amount of $Eu(NO_3)_3 \bullet 5H_2O$ was dissolved in 0.5 mL of water. Different samples were prepared with 0.01; 0.05; 0.06; 0.07; 0.08, and 0.1 mmol of $Eu(NO_3)_3 \bullet 5H_2O$. The resultant solution was agitated for 10 min at room temperature. After that, it was poured into a 10 mL borosilicate vial and put in the Monowave 400 reactor. In 10 min, the mixture reached 120 °C. Once the temperature was reached, it was maintained for various periods of time (1 min, 3 min, 5 min, 10 min, 20 min, 60 min and 120 min). Cooling took an average of 3 min to reach 60 °C. Furthermore, the synthesis of YVO_4 products was extended to include various mixed solvents such as methanol-water, polyethylene glycol (PEG)-water, ethanol-water, and isopropanol-water, as well as different pH (pH = 2, 4, 6, 8, 10, and 12) values for the precursor combinations. The desired pH values are achieved by using nitric acid (HNO_3, Sigma-Aldrich) and sodium hydroxide (NaOH, Sigma-Aldrich) solution ($\geq$98%). The schematic illustration in Fig. 1 shows the different parameters used in the preparation of yttrium orthovanadate. The run product was separated through filtration (quality filter paper, Fisher brand), washed many times with distilled water, and dried at 70 °C in air.

The phase purity and crystallinity were investigated by powder X-ray diffraction (XRD). The XRD patterns were recorded using a Bruker D8 Discover diffractometer operating with CuKα radiation ($\lambda = 1.5406$ Å) in the θ/2θ scan mode in the range of 10°–70° with a step size of 0.04° and an integration time of 1s.

The chemical composition of the particles was determined by energy dispersive X-ray spectroscopy (EDS) using EDAX - Pegasus X4M, while particle size and morphology were studied using the FEI NOVA Nano-SEM 200 scanning electron microscope (SEM). To evaluate the particle size distributions, ImageJ was employed to analyze the particle size of the 100 particles manually chosen from each sample image obtained through SEM, with the exception of the holes. ImageJ may characterize spherical and non-spherical shapes using the longest and shortest diameters, perimeter, projected area, or equivalent spherical diameter.

A homemade portable setup (LED, $\lambda = 310$ nm as excitation source) using a CCS200 spectrometer from Thorlabs was used to measure the photoluminescence of Eu-doped YVO_4 nanoparticles. All characterizations were performed at ambient temperature.

3. Results and discussion

3.1. Phase identification, morphology and distribution analysis

In order to characterize the structure of our compounds, X-ray diffraction (XRD) was performed at room temperature. The X-ray powder diffraction pattern of YVO_4:xEu^{3+} (x = 0.01, 0.05, 0.06, 0.07, 0.08, and 0.1 Eu) samples prepared with a holding time of 60 min are displayed in Fig. 2 a. The diffractograms confirm that our compounds are single-phase and have crystallized in tetragonal structure of YVO_4 with space group *I41/amd* (no. 141). The cell constants are $a = 7.1230$ Å, $c = 6.2910$ Å and $V = 319.19$ Å^3 [34]. All reflections are well consistent with JCPDS 00-016-0250. The absence of unindexed XRD peaks related to other phases suggests that a YVO_4:Eu^{3+} solid solution was formed. The powder XRD patterns of YVO_4:xEu^{3+} (x = 0.01, 0.05, 0.06, 0.07, 0.08, and 0.1 Eu) were refined by the Rietveld method [35] using the FullProf program [36]. Fig. 2 b displays the observed, calculated, and difference curves for the Rietveld refined XRD pattern for the sample corresponding to a 0.07 Eu concentration that was selected as the analysis object.

The goodness values of our samples close to 1 suggest that the refinement was successful, indicating a high level of confidence in the accuracy of the refined crystal structure. The sample was confirmed to be crystallized in a tetragonal structure with the space group *I41/amd* (141). The calculated lattice parameters, *a*, *b*, *c* and the volume *V*, were summarized in Table 1. Notably, the refined parameters are slightly different from the standard data for YVO$_4$, which can be attributed to the introduction of Eu^{3+} ions into the YVO$_4$ lattice. Increasing the concentrations of Eu did not result in any regular changes in lattice parameters. Furthermore, the current samples' axial ratio of *c/b* slightly fluctuates around the value of 0.8832 ± 0.0003.

The average crystallite size of our samples was first estimated from the nonoverlapping and most intense diffraction peak (200) of the XRD data using the Debye Scherrer equation [37]. Crystallite sizes are around 10 nm for YVO$_4$:xEu^{3+} (x = 0.01, 0.05, 0.06, 0.07, 0.08, and 0.1) samples. No substantial lattice strain was expected because low dopant levels were used. The Scherrer equation provided a decent approximation of the size of the crystallites, and it was found that the particle size remained constant despite varying levels of europium doping. This is due to the similarity in radii between the Eu^{3+} ion (with a radius of $r_{Eu^{3+}}$ = 0.95 Å) and the Y^{3+} ion (with a radius of $r_{Y^{3+}}$ = 0.90 Å) [38].

Moreover, the synthesis time does not tend to influence the crystalline structure of the obtained nanoparticles, as shown in Fig. 2 c. This figure depicts the X-ray diffraction patterns of samples obtained after crystallization at different holding times (t = 0 min, 1 min, 3 min, 5 min, 10 min, 20 min, 40 min, 60 min, and 120 min) at a fixed Eu concentration (10 mol%). T = 0 min implies that the sample was produced by simple mixing the precursors without using the microwave process at room temperature. When compared to the 2θ position of the three most intense peaks, corresponding to the (111), (220), and (311) planes, there is no noticeable deviation from the reference patterns for nanoparticles synthesized for different heating hold times at 120 °C. Although no phase transformation occurs as the synthesis holding time increases, the crystallite size increases slightly but remains practically constant at roughly 10 nm, with the exception of the sample obtained at room temperature (t = 0 min), which reaches 5 nm. Specifically, crystallite sizes rise from 8 to 12 nm as hold time increases from 3 to 120 min. This minor increase can be attributed to the low temperature employed in the synthesis (t = 120 °C).

The crystallite size D$_{W-H}$ can also be determined using the Williamson-Hall approach as it effectively separates the size and intrinsic strain broadening by considering peak width as a function of 2θ. These YVO$_4$:xEu^{3+} (x = 0.01, 0.05, 0.06, 0.07, 0.08, and 0.1) samples parameters were calculated using the following equation [39]:

$$\beta = \beta_s + \beta_i = 4\varepsilon \, tan \, \theta + \frac{K\lambda}{D_{W-H} \, cos \, \theta} \tag{2}$$

Where β = FWHM of the XRD peaks, β_i = FWHM without instrumental broadening and β_s = strain broadening.

Equation (2) can be expressed as follows:

$$\beta \, cos \, \theta = 4\varepsilon \, sin \, \theta + \frac{K\lambda}{D_{W-H}} \tag{3}$$

By employing a linear fit model to analyze the curve, specifically, the relationship between 4 sinθ (x-axis) and βcosθ (y-axis) (as depicted in Fig. 3), we effectively calculated ε by extracting the slope of this graph. Simultaneously, we determined the crystallite size D$_{W-H}$ by deriving it from the point where the curve intersects the vertical axis at sinθ = 0. The gathered values are reported in Table 2. As previously highlighted, the crystallite size calculated through the application of the Williamson-Hall model consistently yields slightly larger values compared to those obtained through the utilization of Scherrer's formula. This disparity arises from the inherent limitation of Scherrer's method, wherein it overlooks the broadening effect resulting from the presence of strain, as elucidated in Ref. [40].

SEM microphotographs and the ImageJ processing program were used to evaluate the morphology of the particles and measure the particle size and size distribution of the samples. SEM images of YVO$_4$:Eu^{3+} as-prepared with different concentrations is illustrated in Fig. 4 a. The surface morphology of the phosphor is significantly affected by Eu^{3+}-doping in the host YVO$_4$. The phosphor crystallizes as petal-like particles at low Eu concentrations, with particle sizes of 45 nm and 39 nm at 0.01 and 0.05 concentrations, respectively (see Fig. 4b). The particle size of the samples generated with low concentrations of Eu (0.01 and 0.05) is clearly larger than the particle size estimated by the Debye-Scherrer method. This is due to the fact that each grain is made up of agglomerated crystallites. Meanwhile, when the Eu^{3+}-doping was increased from x = 0.06 to 0.1, there was a decrease in the agglomeration and the grains became smaller, which suggests that a higher amount of dopant contributes to the formation of nanoparticles with higher surface energy. Moreover, the particles with more dopant appear to be distributed in a more dispersed manner indicating that the amount of dopant may affect both the degree of aggregation and particle size. The particle size distribution of each sample and the mean sizes are indicated in Fig. 4 b. The particles clearly have spherical morphologies with highly homogeneous size distributions around 25 nm, which can be useful for some applications, such as latent fingerprint imaging [41].

Fig. 5 presents the SEM images of YVO$_4$: 0.1Eu^{3+} nanophosphors synthesized at different holding times at 120 °C. These values, which rise from 12 nm for t = 0 min to 35 nm for t = 120 min, are considerably higher than those obtained by XRD, owing to crystallite aggregation. These results show an effective method for particle size control by simply adjusting the time for crystallization at a constant temperature.

The EDS spectra relative to the YVO$_4$:xEu^{3+} (x = 0.01; 0.07 and 0.1) samples, shown in Fig. 6, reveal the existence of all elements (oxygen (O), vanadium (V), yttrium (Y), and europium (Eu)) close to the stochiometric proportions, and confirm the incorporation of Eu atoms into
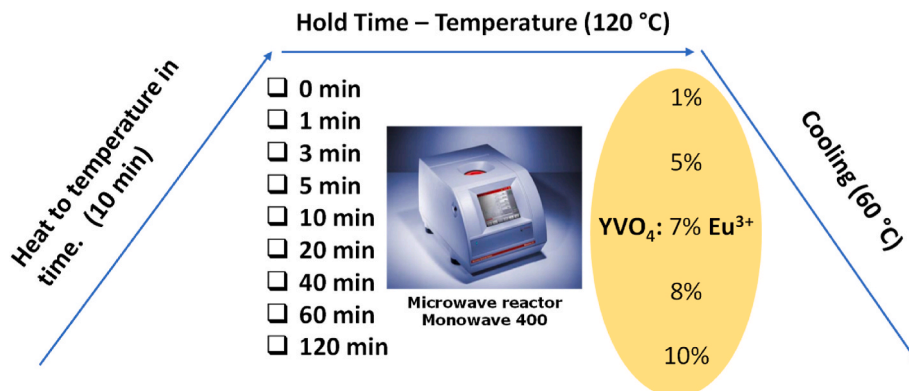

Fig. 1. Schematic illustrates the different concentrations of doped Eu^{3+} in the YVO$_4$ nanoparticles and the different heating times via a microwave-assisted process.

the yttrium orthovanadate structure. Weight (%) and atomic (%) of constituent elements in synthesized nanocrystalline materials are reported in the inset of Fig. 6, which is in good accord with the concentration of dopant ion incorporated during their synthesis. The mole ratio of Eu^{3+} and Y^{3+} was slightly higher than the expected value (for x = 0.1, the ratio Eu^{3+}/Y^{3+} equals 0.12).

The dynamic behavior of our material systems in aqueous solutions was studied using dynamic light scattering (DLS), which was used to evaluate the size distribution profile of small particles in suspension and the zeta potential. The polydispersity index (PDI) corresponding to our samples is close to zero, indicating a monodisperse system characterized by particles with a very narrow size distribution and minimal size variation. The 0.07 doping level yields the minimum PDI value, which can be considered an important factor in attaining the desired properties and optimal performance.

In terms of zeta potential, it is well recognized that nanoparticles with zeta potential values close to neutrality, in fact between −25 and + 25 mV, are unstable in aqueous suspensions, while nanoparticles with zeta potential values more negative than −25 mV or more positive than +25 mV exhibit moderate stabilities due to charge repulsion [42]. The zeta potential was registered for YVO₄:xEu (x = 0.01, 0.05 … and 0.1), indicating that the dispersed particles in the suspension are positively charged. Furthermore, the resulting nanoparticles' zeta potential (+34 mV) assures a high degree of stability for the nanosuspension, while lower zeta potential values will eventually agglomerate owing to Van Der Waal inter-particle attractions [42]. The zeta potential of yttrium orthovanadate doped europium increases with increasing Eu concentration, as seen in Table 3. The Z-average size measured by DLS are also presented in Table 3, which are clearly bigger than the crystallite sizes, due to some particle's aggregation. The increase in Eu concentration led to a decrease in the average particle size. This observation aligns with the SEM images, which provide evidence that the incorporation of Eu^{3+} into the YVO₄ host effectively reduces particle agglomeration. Colloidal stability in aqueous suspensions and low aggregation of nanoparticles are required for potential biological applications [43]. According to our results, the average zeta potential of the aqueous colloidal solution of YVO₄:Eu^{3+} was determined to be 34 mV, which confirms good stability [44].

3.2. Impact of Eu concentration on the optical properties of YVO₄: xEu³⁺

The doping concentration of the luminescence centers, as is well known, has a significant impact on the performance of the phosphors. Therefore, it is necessary to confirm the appropriate doping concentration to achieve maximum luminescence intensity.

The excitation spectra of YVO₄:0.1Eu³⁺ sample (Fig. 7) has a large absorption band with a high peak at 308 nm, which may be attributed to charge transfer from the oxygen ligands (O^{2-}) to the central vanadium atom (V^{5+}) inside the VO_4^{3-} groups [45,46]. Additionally, some weak bands are located in the 360-400 nm wavelength range, including 381 nm ($^7F_0 \rightarrow {}^5L_7$) and 395 nm ($^7F_0 \rightarrow {}^5L_6$). The sharp excitation band at 395 nm is attributed to the intra-configurative f-f transitions of Eu^{3+} ions in the host lattice [47].

In order to determine the optimal concentration corresponding to the maximum luminescence at 619 nm, we have investigated a series of YVO₄:xEu³⁺ products with different Eu^{3+} concentrations (x = 0.01; 0.05; 0.06; 0.07 and 0.1). Under the same experimental conditions, the emission spectra of all samples with varying doping amounts at two different hold times (T = 20 min and T = 60 min) were measured upon 310 nm excitation. The integrated emission intensity of the $^5D_0 \rightarrow {}^7F_i$ (i = 1, 2, 3, 4) transitions were evaluated for all samples, and the dependence of the maximum luminescent intensity on Eu^{3+} concentration is plotted in Fig. 8 a. From the comparison of the data sets, it is apparent that the intensities of the emission transitions gradually increase with increasing Eu^{3+} ion concentration and reach a maximum at x = 0.07, and then drop with increasing the concentration. This effect is owing to the well-known phenomenon of concentration quenching in rare earth-doped systems as a result of mutual Eu^{3+}- Eu^{3+} interactions [47]. The particle morphology appears unchanged by increasing doping with Eu^{3+} concentrations. In the case, a small increase of the crystallite size with the dopant concentration was accompanied by a reduction of the particle size, showing that the amount of dopant may affect both the degree of aggregation and particle size. Apparently, the optimal Eu^{3+} concentration corresponds to x = 0.07 (inset of Fig. 8a). This result is consistent with the findings of Liu et al. [47].

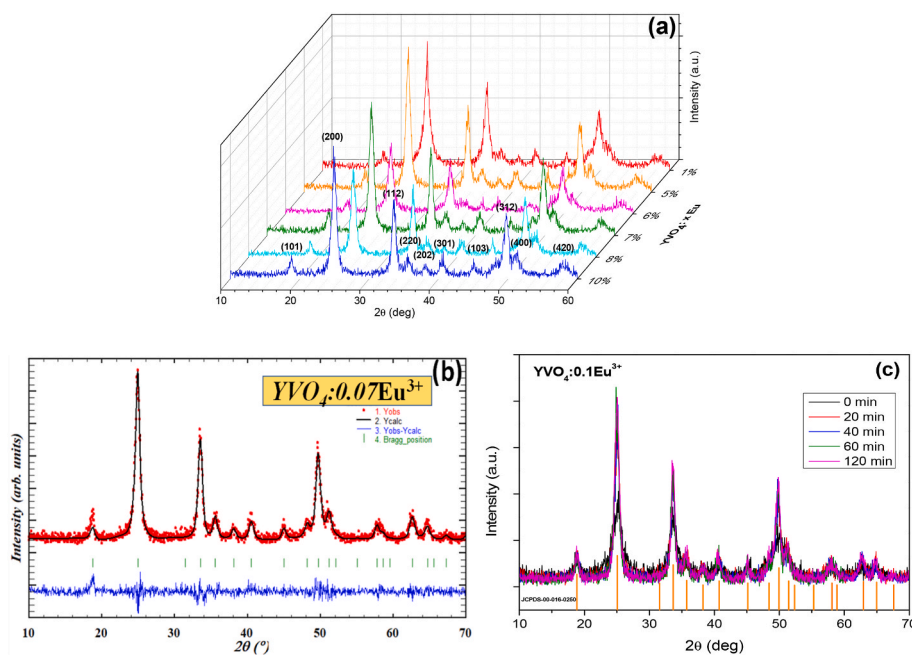In general, the two main aspects of the resonance electronic excita-

Fig. 2. XRD patterns and standard card of YVO₄ (JSPDS 016-0250) of **(a)** the concentration series **(b)** Rietveld data fit on powder X-ray diffraction data for YVO₄:0.07Eu³⁺ nanocrystals. The differential pattern between simulated and experimental data is also displayed. **(c)** XRD patterns of YVO₄:0.1Eu³⁺ with different heating hold times.

Table 1
Refinement results and crystal structure data for the YVO$_4$:xEu (x = 0.01; 0.05; 0.06; 0.07; and 0.1) series were compared with the reference standard of YVO$_4$ (space group *I41/amd*, JCPDS 1-0250).

Parameters	YVO$_4$ PDF#16-0250	YVO$_4$:xEu^{3+}					
	0.00	0.01	0.05	0.06	0.07	0.08	0.1
a = b (Å)	7.1230	7.1250	7.1300	7.1370	7.1270	7.1080	7.1320
c (Å)	6.2910	6.2900	6.2950	6.2970	6.2950	6.2830	6.2910
c/b	0.8832	0.8828	0.8828	0.8823	0.8832	0.8839	0.8820
V (Å^3)	319.19	319.28	319.98	320.73	319.77	317.44	319.95
Space group	I41/amd (141)						
GoF	–	1.18	1.14	1.25	1.16	1.27	1.32
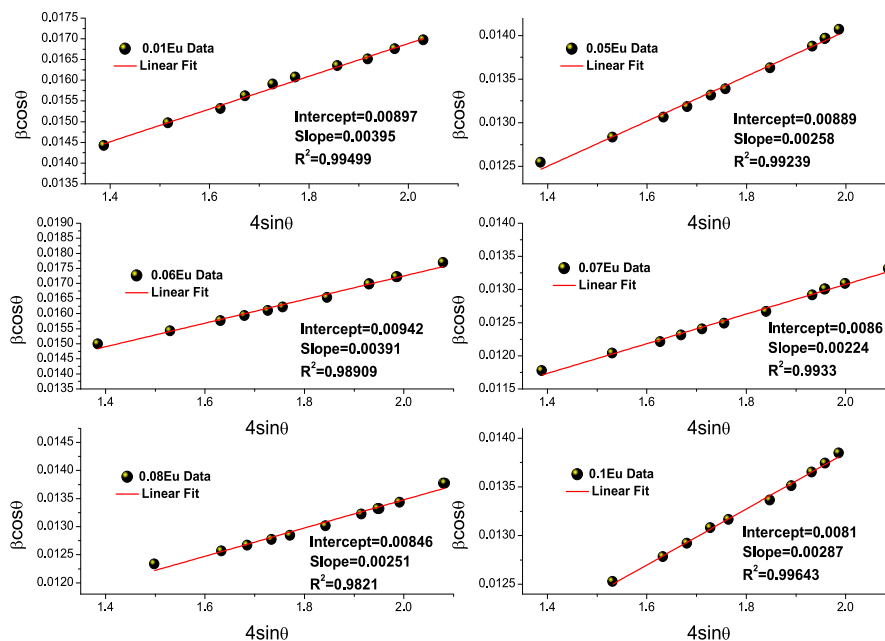
Fig. 3. Size-strain plot for YVO$_4$:xEu^{3+} (x = 0.01, 0.05, 0.06, 0.08, and 0.1) samples.

Table 2
Crystallite size (D$_{W-H}$) and strain (ε) of the YVO$_4$:xEu^{3+} (x = 0.01, 0.05, 0.06, 0.07, 0.08 and 0.1) samples calculated by Williamson-Hall method.

Composition (x)	Strain ε (10^{-3})	Crystallite size D$_{W-H}$ (nm)
0.01	2.872	15.5
0.05	1.878	15.56
0.06	2.849	14.7
0.07	1.877	16.1
0.08	2.094	16.4
0.1	2.092	17.1

tion energy transfer mechanism are the exchange interaction (Dexter) [48] and the electric dipolar interaction (Forster) [49–51]. The exchange interaction is a short-distance interaction, with a typical critical distance R$_C$ of about 5 Å, whereas the critical distance of the diploar interaction can be as high as 410 Å [52]. Increasing the concentration of active center (Eu^{3+} ions) promotes energy transfer while decreasing the cross-relaxation change distance between neighboring Eu^{3+} defects, resulting in non-radiative recombination and decreased efficiency. As a consequence, the emission strength peaks at a balance point, which we consider the "concentration quenching effect". Therefore, the critical distance R$_C$ is used to describe the distance between Eu^{3+} ions when quenching occurs. According to Blasse's suggested mechanism, the R$_C$ can be defined as follows [53]:

$$R_C = 2\left(\frac{3V}{4\pi X_c N}\right)^{1/3} \qquad (4)$$

where V is the volume of the crystallographic unit cell, X$_C$ is the critical concentration, and n is the number of lattice sites that the activator ions can occupy. The determined critical distance for the system YVO$_4$:Eu^{3+} is approximately 12.96 Å, which corresponds to the YVO$_4$ host lattice, V = 319.19 Å^3, N = 4, and X$_C$ = 0.07. The obtained value of R$_C$ is much larger than 5 Å, suggesting that energy transfer via the exchange mechanism is less likely. Therefore, the energy transfer of Eu^{3+} is mainly via the electrical interaction [48].

Meanwhile, the optimal concentration of doped Eu^{3+} in the host YVO$_4$ produced at 20 min was examined. According to the results in Fig. 8 b, the optimum concentration is x = 0.10. Notably, the PL intensity of Eu^{3+} increases progressively with concentration for samples obtained with a holding time of 20 min.

As a measure, for a synthesis temperature of 120 °C, the maximum emission intensity in YVO$_4$ nanoparticles corresponding to the optimal Eu doping concentration (x = 0; 0.05; 0.06; 0.07; 0.08 and 0.1) was x = 0.07 and x = 0.10 for temperature holding times of 60 and 20 min, respectively.

3.3. Effect of heating hold time on the PL properties

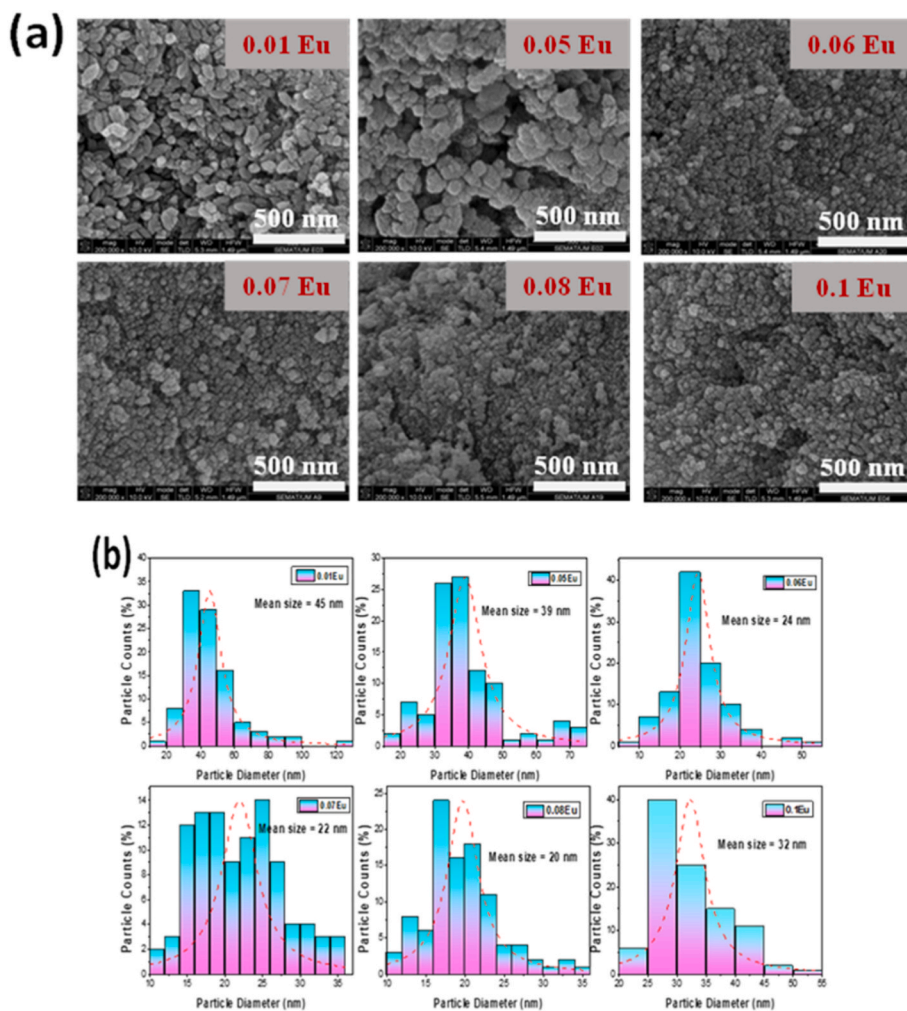The PL spectra of generated nanoparticles YVO$_4$:0.1Eu^{3+} with

Fig. 4. (a) SEM images of YVO$_4$:xEu^{3+} phosphors with different concentrations, a heating holding time of 60 min at 120 °C. **(b)** Shows the particle size distributions.
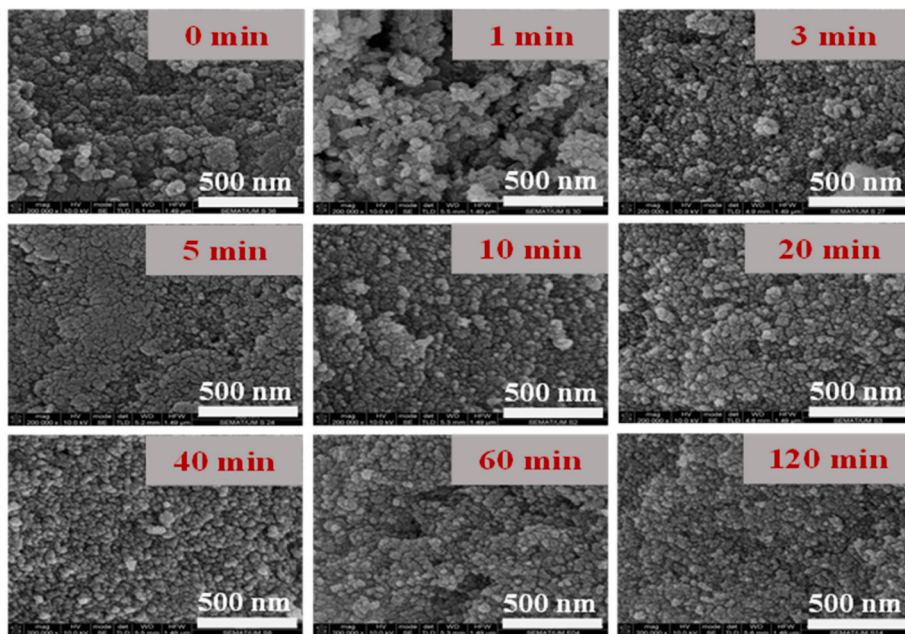

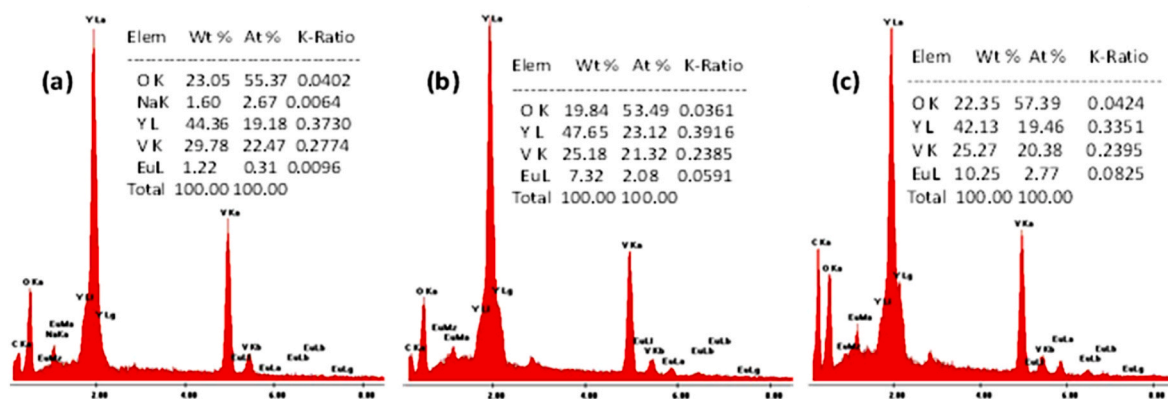**Fig. 5.** SEM images of YVO$_4$:0.1Eu^{3+} phosphors with varying heating hold times at 120 °C.

Fig. 6. The chemical elements in YVO$_4$ nanoparticles doped with Eu^{3+} were analyzed using EDS. The Eu concentrations varied at x = 0.01, 0.07, and 0.1, represented as **(a)**, **(b)**, and **(c)**, respectively.

Table 3

Zeta potential (Z-potential), the average size (Z-average) and Polydispersity index (PDI) of YVO$_4$:xEu^{3+} assayed by dynamic light scattering (DLS).

Samples	Zeta Potential (mV)	Size average (nm)	Polydispersity index
YVO$_4$:0.01Eu^{3+}	34 (5)	296 (75)	0.25
YVO$_4$:0.05Eu^{3+}	38 (9)	154 (82)	0.24
YVO$_4$:0.06Eu^{3+}	36 (0)	183 (14)	0.22
YVO$_4$:0.07Eu^{3+}	35 (1)	112 (16)	0.14
YVO$_4$:0.08Eu^{3+}	37 (2)	100 (05)	0.24
YVO$_4$:0.1Eu^{3+}	43 (8)	87 (42)	0.19
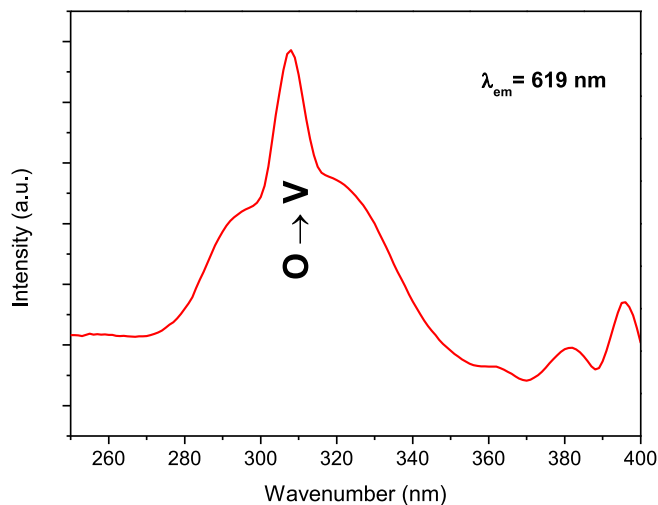
Fig. 7. Excitation spectrum of YVO$_4$:0.1Eu^{3+} sample.

Fig. 8. Emission spectra of the PL nanoparticles (YVO$_4$: xEu) with x = 0.01; 0.05; 0.06; 0.07; 0.08 and 0.1 at two distinct hold times t = 60 min **(a)** and t = 20 min **(b)** (λ_{ex} = 310 nm).

different hold times, under 310 nm excitation, are exhibited in Fig. 9. These spectra demonstrate the capability of the YVO$_4$ host to absorb the 310 nm excitation wavelength and efficiently transfer the energy to the Eu^{3+} activators.

Under UV excitation, The YVO$_4$:0.1Eu^{3+} emits strong red luminescence with narrow bands corresponding to $^5D_0 \rightarrow {}^7F_i$ (i = 1, 2, 3, 4) Eu^{3+} intra-4f transitions. The two most intense peaks at 619 nm and 622 nm correspond to the $^5D_0 \rightarrow {}^7F_2$ forced electric dipole transitions, as explained by Judd-Ofelt theory [54]. This theory suggests that the dominant emission in the 600-630 nm range is caused by the partially allowed electric-dipole transition $^5D_0$–$^7F_2$ of Eu^{3+} due to the absence of an inversion center (D$_{2d}$ symmetry). Previous research on similar nanoparticles has also shown that the spectra are primarily dominated by the emission from europium ions, specifically the $^5D_0 \rightarrow {}^7F_{2,4}$
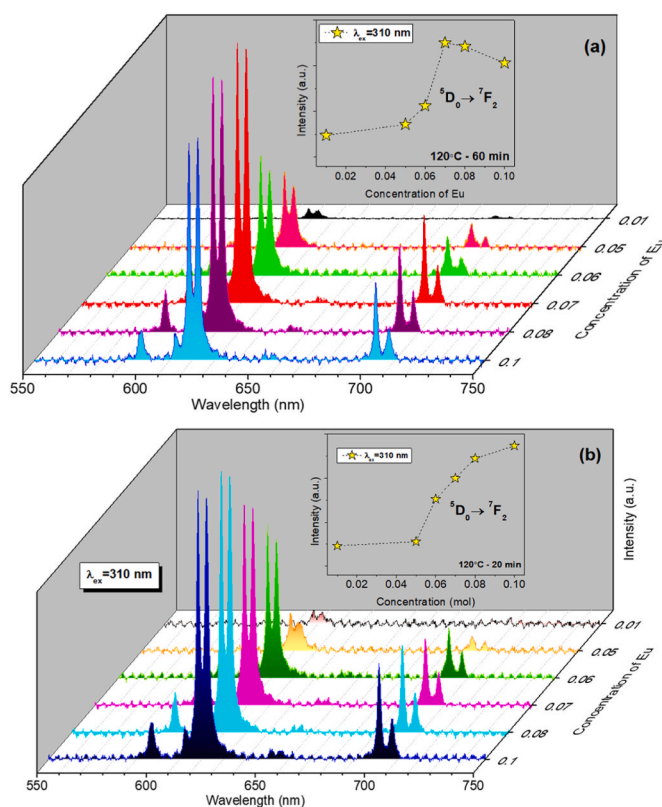
(electric-dipole transitions), which can be attributed to the absence of an inversion symmetry at the europium site [55]. Meanwhile, the weak peaks at 594, 652, and 702 nm are consistent with the transitions of $^5D_0 \rightarrow {}^7F_1$, $^5D_0 \rightarrow {}^7F_3$, and $^5D_0 \rightarrow {}^7F_4$, respectively. The detected transitions of $^5D_0 \rightarrow {}^7F_{1,3}$ were correlated with the magnetic dipole transitions. Furthermore, we notice that the emission intensity increases with the increasing of the hold time. Obviously, the $^5D_0 \rightarrow {}^7F_2$ electric dipole transition is a hypersensitive transition, which is only allowed if the europium ion occupies a site without an inversion center and is, therefore, very sensitive to the local environment [56]. Comparing the PL curves, it is clear that the intensities of the emission transitions reach their maximum at 120 min, as indicated in the inset of Fig. 9. Thus, with increasing heating time, the luminescence intensity of the samples
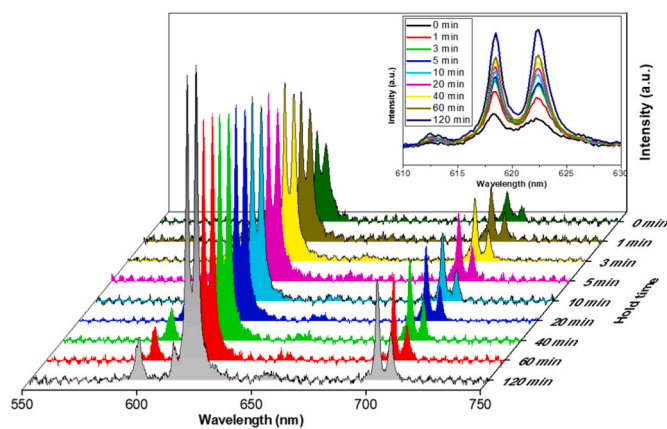
Fig. 9. The PL spectra of YVO$_4$:0.1Eu^{3+} nanoparticles with various hold times at 310 nm excitation wavelength. The inset indicates the evolution of the electronic transition intensity with heating hold times.

increases accordingly. As a result of the lack of inversion symmetry surrounding the Eu^{3+} ion, the majority of the emission occurs at the hypersensitive $^5D_0 \rightarrow {}^7F_2$ electric dipole transition, giving the material an intense red emission.

The luminescence is clearly enhanced as the nanoparticle dimensions (crystallite size and particle size) rise with hold (synthesis) time at 120 °C, ranging from 12 nm to 35 nm suggesting that also the lower density of defects per surface area contribute to higher emission. With the increasing synthesis temperature, an increase of crystallite size and of particle size were found, together with an increase of the photoluminescence intensity. This suggests that with the temperature a better-ordered crystal phase was achieved, resulting in a higher luminescent intensity.

3.4. Influence of temperature on the PL properties

To investigate the influence of temperature on PL properties, we prepared YVO$_4$:0.1Eu^{3+} by the hydrothermal method as described above (the holding time is set at 20 min) at 150, and 180 °C. In Fig. 10, all of the diffraction peaks for our nanoparticles can be easily indexed as the YVO$_4$ tetragonal phase (JCPDS, No. 00-016-0250), confirming that all of the particles maintained highly crystalline structures with no additional impurity phases. Using the Debye Scherrer equation, the average crystallite size of the samples synthesized at 120, 150, and 180 °C was determined to be 9, 10, and 13 nm, respectively. In addition, the morphology of the analyzed samples was examined using a SEM, as
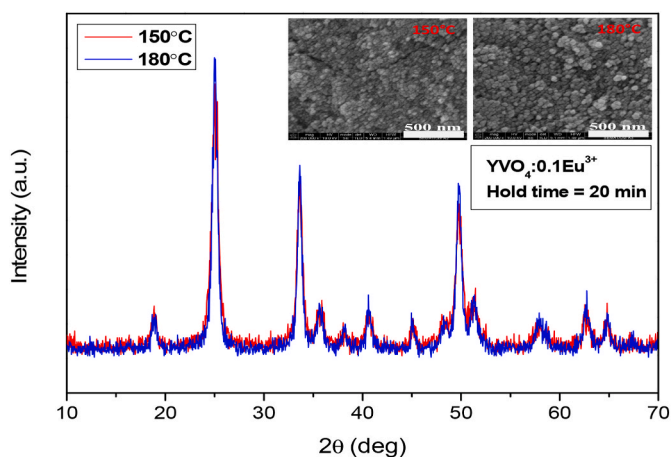
shown in the inset of Fig. 10, and the average particle size was determined. The SEM images reveal the presence of homogeneous nanoparticles with spherical shapes, exhibiting a narrow size distribution. Luminescence intensity is one of the properties that can be influenced by the shape and size of the particles [29], and spherical particles can lead to increased photoluminescence. This is due to the fact that light scattering is modest in a spherical sample, but the packing density is significantly larger than in others [57]. According to Vini et al. [58], the Y$_2$O$_3$:Eu^{3+} nanoparticles have a spherical form and a small particle size, making them suitable for laser materials, phosphors, and optoelectronic devices [57].

The particle size of samples increases as the synthesis temperature (120-180 °C) rises. The average sizes of the particles synthesized at 120, 150, and 180 °C are about 13, 17, and 30 nm, respectively. Fig. 11 depicts the effect of synthesis temperatures on the PL emission intensities of YVO$_4$:0.1Eu^{3+} samples. The maximum intensity of our samples developed as the temperature increased, suggesting the electronic transition's sensitivity to its surroundings. Furthermore, as illustrated in the inset of Fig. 11, the PL intensity of the as-prepared samples follows an increasing trend with increasing synthesis temperatures from 120 °C to 180 °C. The $^5D_0 \rightarrow {}^7F_2$ transition is widely recognized to be extremely susceptible to structural changes and environmental impacts [45]. The larger particles generally show a smaller surface-to-volume ratio and, thus, fewer surface defects, which can enhance the luminescent intensity.

3.5. Impact of water quantity on the PL properties

The YVO$_4$:0.07Eu^{3+} samples were prepared under the same conditions as previously stated (the holding period was set at 20 min), with a fixed amount of precursors but varying volumes of water (2, 3, 4, 5, and 10 mL). Fig. 12 a shows XRD patterns of the samples synthesized at given water values. All diffraction patterns matched well the standard diffraction data for bulk YVO$_4$ (JCPDS, No. 00-016-0250). The crystallinity of the samples is also high, as evidenced by sharp diffraction peaks. According to the Debye Scherrer equation, the nano-crystallite size of YVO$_4$:0.07Eu^{3+} was approximately 7, 8, 8, 10, and 10 nm at varying volumes of water (2, 3, 4, 5, and 10 mL, respectively). As a result, the amount of water added during preparation has little impact on particle size growth. As the amount of water used in the synthesis increase, the particle sizes changed in accordance, as illustrated in Fig. 12 b. Particularly, 2 ml, 3 ml, 4 ml, 5 ml, and 10 ml of water in the synthesis resulted in particle sizes of 14 nm, 15 nm, 16 nm, 20 nm, and
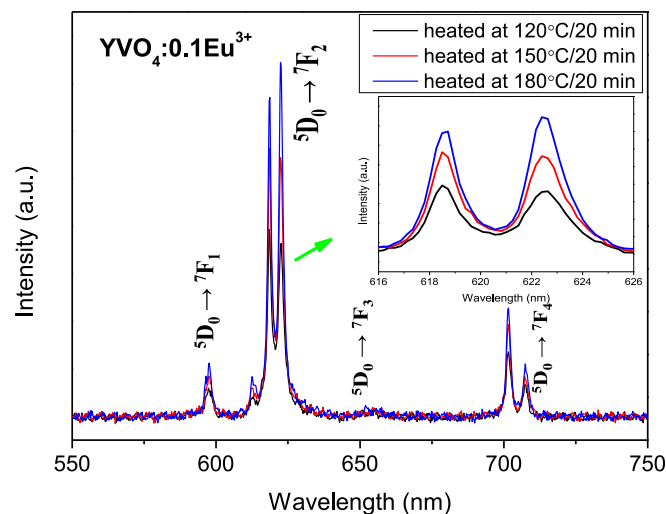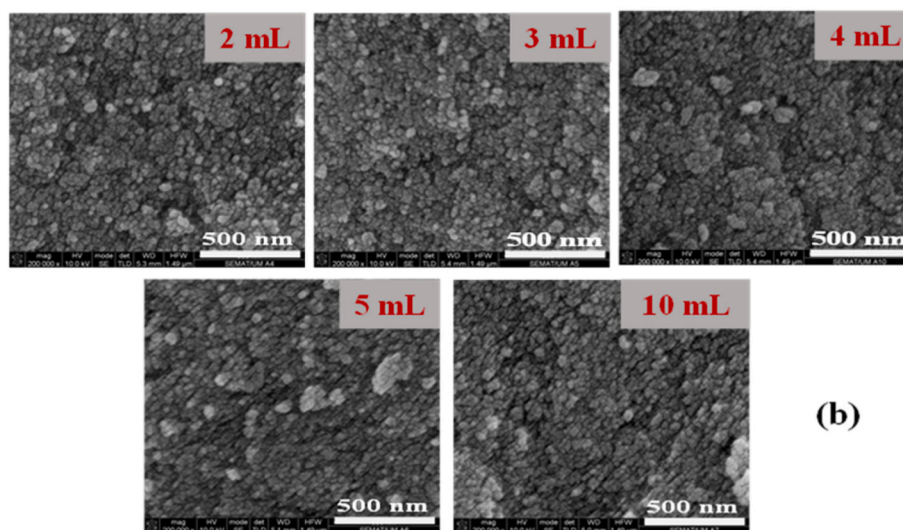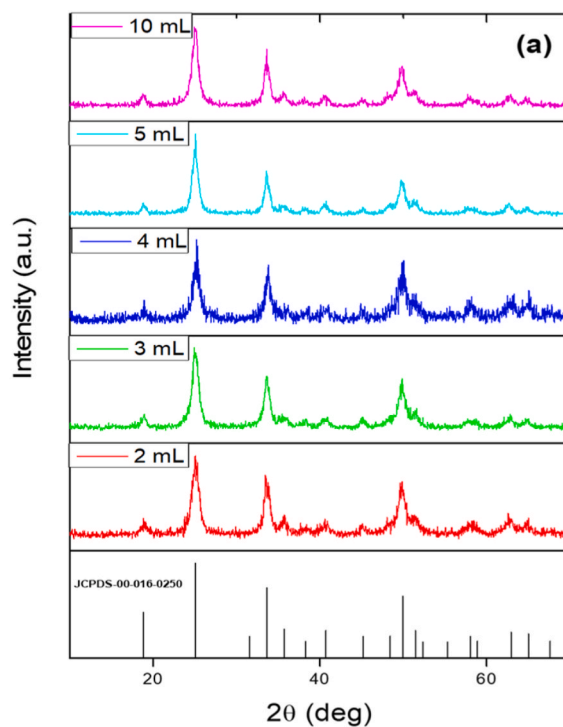

Fig. 10. XRD patterns of YVO$_4$:0.1Eu^{3+} synthesized at 150 and 180 °C. The insert represents the SEM images.

Fig. 11. Emission spectra of the PL nanoparticles YVO$_4$: :0.1Eu^{3+} at 310 nm excitation wavelength.

Fig. 12. (a) XRD patterns of europium doped yttrium – orthovanadate nanopowder prepared by microwave with different amounts of water; **(b)** SEM images of $YVO_4:Eu^{3+}$.

18 nm, respectively.

The emission spectra of $YVO_4:0.07Eu^{3+}$ obtained using different volumes of water under excitation at 310 nm are shown in Fig. 13, and are composed of several emission lines in the range 550–750 nm, which originate from the Eu^{3+} activator transitions $^5D_0$-^7F_J (J = 1, 2, 3, 4). The emission spectrum exhibited a consistent pattern across all samples prepared. Clearly, the PL intensity of Eu^{3+} steadily increases when the amount of water increases to 5 mL (inset Fig. 13) and subsequently decreases when the volume of water exceeds 5 mL due to quenching. The morphology of the $YVO_4:0.07Eu^{3+}$ remains unaffected by the varying volumes of water used during processing; however, there is a slight impact on the growth of particle size.

3.6. The implications of changing the pH value and solvent

In order to investigate the effect of pH on the PL properties, $YVO_4:0.07Eu^{3+}$ samples were produced at different pH ranges using water as a solvent. The pH value of the prepared $YVO_4:0.07Eu^{3+}$ suspension with only water is 6. The pH range of 2–12 was achieved by adjusting a solution using a high-purity sodium to create an alkaline environment, while an acidic solution was obtained by utilizing 70% concentrated nitric acid. As illustrated in Fig. 14, the pH values of the precursor solution have a considerable influence on the luminescent intensity of the final products. The luminous intensity of the principal peaks decreased as the acidity or alkalinity of the $YVO_4:0.07Eu^{3+}$ solution increased, indicating that the maximum intensity occurred at pH value of 6. The intensity of the emission spectra decreased steadily as the pH increased from 6 to 12. This effect may be explained by the fact that
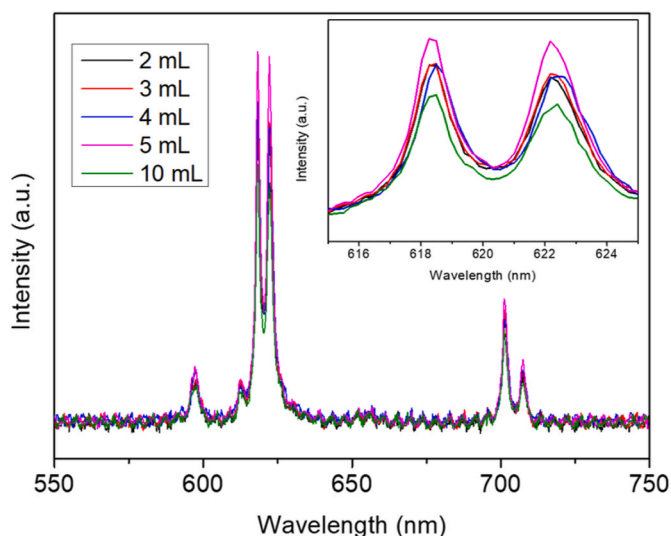
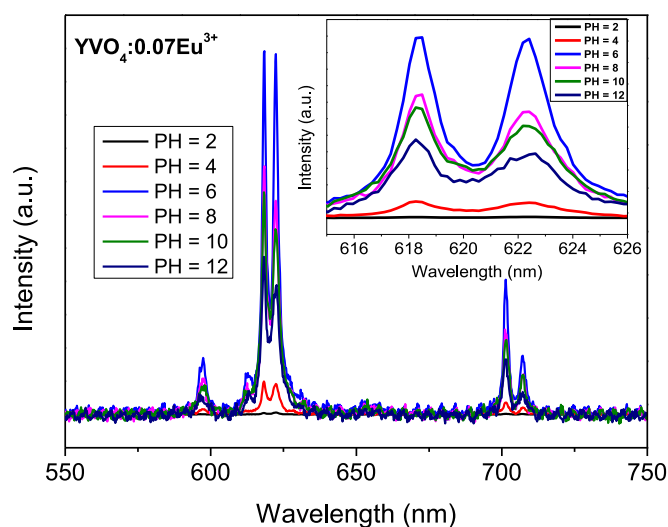**Fig. 13.** Emission spectra of YVO$_4$: 0.07Eu^{3+} with varying amounts of water.

Fig. 14. PL spectra of YVO$_4$:0.07Eu^{3+} collected at different pH values of the solution (pH = 2, 4, 6, 8, 10, 12) at 310 nm excitation wavelength.

the particles were scattered in water and their surfaces were covered by a large number of OH groups that were either chemically linked to the surface or simply adsorbed as water molecules. Such hydroxyl groups are particularly efficient quenchers of lanthanide luminescence via multiphoton relaxation [59]. Numerous studies in the literature have explored the optimization of emission intensity by manipulating pH values. These studies have demonstrated that, although high emission intensities can be achieved, they vary across different pH values [36,60, 61]. As mentioned earlier, the pH that resulted in the highest luminescence differed from the values reported by other researchers, suggesting the presence of several important factors, including chemical precursors, solvents, and preparation methods, that may be responsible for the observed variations [62].

Fig. 15 a shows the PL spectra of the Eu^{3+}-doped YVO$_4$ samples produced in various solvents. The emission spectra of the products synthesized in different solvents differ mainly by their peak intensity, demonstrating that the luminescent properties are closely related to the agglomeration of particles. On the basis of the above SEM images indicated in Fig. 15 b, there is an obvious agglomeration to form large particles when.
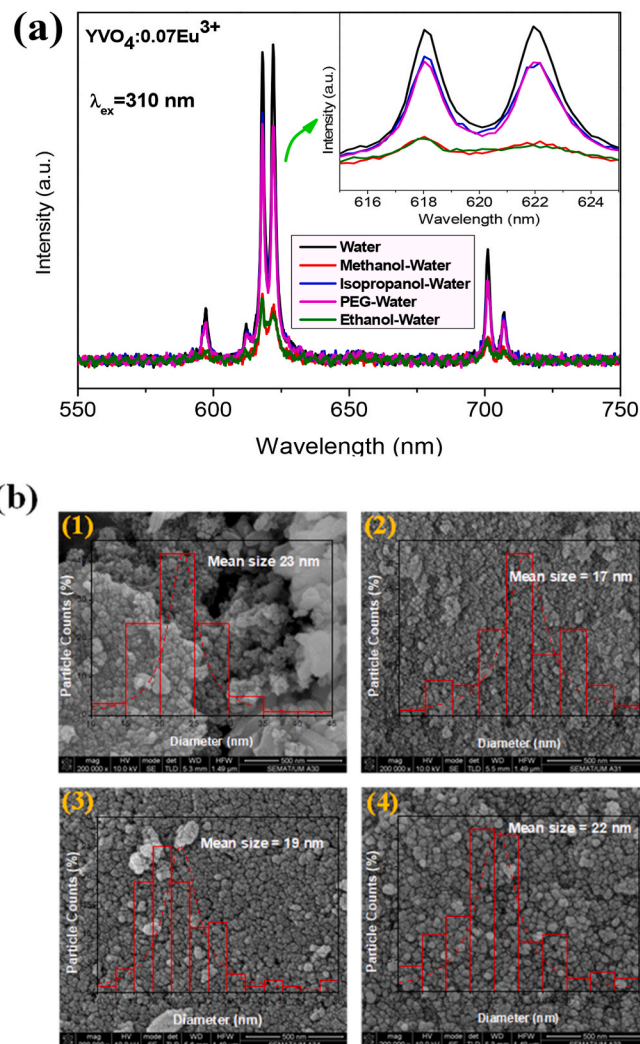

Fig. 15. (a) Emission spectra of YVO$_4$:0.07Eu^{3+} nanoparticle obtained with several solvents: (1) methanol-water, (2) isopropanol-water, (3) ethanol-water, and (4) PEG-water. **(b)** SEM photographs of YVO$_4$:0.07Eu^{3+} crystals prepared under various solvents at the above, respectively and their particle size distributions.

using ethanol-water and methanol-water as solvents, which results in a significant drop in emission intensity. On the other hand, the use of isopropanol-water and PEG-water as solvents reduces the agglomeration of nanoparticles and makes them appear well dispersed, which enhances the luminosity but is still lower than green solvent (only water). Liu et al. [36] tested various types of mixed solvents to enhance the luminescence intensity of Eu^{3+}-doped in the YVO$_4$ host, demonstrating that the ethanol-water solvent is the most effective. In the present instance, using only water as the solvent was sufficient to obtain the highest emission intensity for YVO$_4$:0.07Eu nanoparticle.

4. Conclusions

In summary, this work shows optimized microwave synthesis of phase pure red-emitting YVO$_4$:Eu^{3+} phosphor. The experimental data revealed that the physicochemical conditions (microwave heating time, quantity of water, pH values of solution and dopant concentration) significantly impacted the particle size and distribution. The initial synthesis suspension with pH of 6 containing only water as a solvent yielded the samples with the highest emission intensity. The PL spectra of YVO$_4$:Eu^{3+} indicated that different particle sizes and Eu concentrations influence the optical properties. The obtained particles show

intense red luminescence with narrow bands corresponding to $^5D_0$-^7F_j intra-4f transitions (j = 1, 2, 3, 4) Eu^{3+}, with the strongest at 619 nm. The highest emission intensity in YVO_4:xEu nanoparticles, corresponding to the optimal doping concentration of Eu (x = 0.01; 0.05; 0.06; 0.07; 0.08 and 0.1), was 0.07 for temperature holding times of 60 min. The critical distance, R_C, of Eu^{3+} energy transfer is 12.96 Å, calculated by the concentration quenching method. Based on their nanoparticles size, morphology and luminescent properties, the Eu^{3+}-doped YVO_4 samples are potential materials for application in UV radiation detectors and light-emitting phosphors.

Credit author statement

H. E. Sekrafi: Design, Methodology, Investigation Data Analysis, Software, Writing.

E. Hergli: Visualization, Data Analysis, Investigation.

S. Ferdov: Design, Data curation supervision, Methodology, Validation, Reviewing and Editing.

P. Coutinho: Design, Reviewing and Editing.

A. Mota: Conceptualization, Validation.

J. Lopes: Conceptualization, Validation.

L. Rebouta: Supervision, Resources, Reviewing and Editing.

Declaration of competing interest

The authors declare that they have no known competing financial interests or personal relationships that could have appeared to influence the work reported in this paper.

Data availability

Data will be made available on request.

Acknowledgements

References

[1] M. Yu, J. Lin, Z. Wang, J. Fu, S. Wang, H.J. Zhang, Y.C. Han, Fabrication, patterning, and optical properties of nanocrystalline YVO_4:A (A = Eu^{3+}, Dy^{3+}, Sm^{3+}, Er^{3+}) phosphor films via Sol–Gel soft lithography, Chem. Mater. 14 (2002) 2224–2231, https://doi.org/10.1021/cm011663y.

[2] Amit K. Vishwakarma, Kaushal Jha, M. Jayasimhadri, Enhancement of luminescent properties in Eu^{3+} doped $BaNb_2O_6$ nanophosphor synthesized by facile metal citrate gel method, Opt. Mater. 96 (2019), 109301, https://doi.org/10.1016/j.optmat.2019.10930.

[3] Y.H. Zhou, J. Lin, Luminescent properties of YVO_4:Dy^{3+} phosphors prepared by spray pyrolysis, J. Alloys Compd. 408 (2006) 856–859, https://doi.org/10.1016/j.jallcom.2004.11.085.

[4] M. Shokouhimehr, Prussian Blue Nanoparticles and its Analogues as New–Generation T1-Weighted MRI Contrast Agents for Cellular Imaging, Kent State University, 2010.

[5] V.P. Hedaoo, V.B. Bhatkar, S.K. Omanwar, Combustion synthesis and photoluminescence in novel red emitting yttrium gadolinium pyrosilicate nanocrystalline phosphor, J. Alloys Compd. 672 (2016) 653–659, https://doi.org/10.1016/j.jallcom.2016.02.203.

[6] G. Jia, C.M. Zhang, S.W. Ding, L.Y. Wang, L.F. Li, H.P. You, Synthesis and enhanced luminescence of uniform and well-dispersed quasispherical YVO_4:Ln^{3+} (Ln = Eu, Dy) nanoparticles by a solvothermal method, CrystEngComm 14 (2012) 573–578, https://doi.org/10.1039/C1CE05725A.

[7] N. Venkatachalam, E. Hemmer, T. Yamano, H. Hyodo, H. Kishimoto, Synthesis and toxicity assay of ceramic nanophosphors for bioimaging with near-infrared excitation, Prog. Cryst. Growth Char. 58 (2012) 121–134, https://doi.org/10.1016/j.pcrysgrow.2012.02.002.

[8] C. Brecher, H. Samelson, A. Lempicki, R. Riley, T. Peters, Polarized Spectra and crystal-field parameters of Eu^{3+} in YVO_4, Phys. Rev. 155 (1967) 178, https://doi.org/10.1103/PhysRev.155.178.

[9] L. Tong, J. Shi, D. Liu, Q. Li, X. Ren, H. Yang, Luminescent and magnetic properties of Fe_3O_4@SiO_2@Y_2O_3:Eu^{3+} composites with Core−Shell structure, J. Phys. Chem. C 116 (2012) 7153–7157, https://doi.org/10.1021/jp212579t.

[10] H. Li, Q. Deng, B. Liu, J. Yang, B. Wu, Fabrication of core@spacer@shell Aunanorod@mSiO_2@Y_2O_3: Er nanocomposites with enhanced upconversion fluorescence, RSC Adv. 6 (2016) 13343–13348, https://doi.org/10.1039/C5RA23884F.

[11] S. Faria, E. Mehalchick, YVO_4: Eu, Tb—an Efficient high pressure mercury vapor lamp phosphor, J. Electrochem. Soc. 121 (1974) 305–307, https://doi.org/10.1149/1.2401802.

[12] M.N. Luwang, R.S. Ningthoujam, S.K. Srivastava, R.K. Vatsa, Preparation of white light emitting YVO_4: ln3+ and silica-coated YVO_4:Ln3+ (Ln3+ = Eu3+, Dy3+, Tm3+) nanoparticles by CTAB/n-butanol/hexane/water microemulsion route: energy transfer and site symmetry studies, J. Mater. Chem. 21 (2011) 5326–5337, https://doi.org/10.1039/C0JM03470C.

[13] Didier Casanova, Cédric Bouzigues, Thanh-Liêm Nguyên, Rivo O. Ramodiharilafy, Latifa Bouzhir-Sima, Antigoni Alexandrou, Single europium-doped nanoparticles measure temporal pattern of reactive oxygen species production inside cells, Nat. Nanotechnol. 4 (2009) 581–585, https://doi.org/10.1038/nnano.2009.200.

[14] L.E. Shea, J. Mckittrick, O.A. Lopez, Synthesis of red emitting, small particle size luminescent oxides using an optimized combustion process, J. Am. Ceram. 79 (1996) 3257–3265, https://doi.org/10.1111/j.1151-2916.1996.tb08103.x.

[15] M. Shokouhimehr, S.M. Rafiaei, Combustion synthesized YVO_4:Eu^{3+} phosphors: effect of fuels on nanostructure and luminescence properties, Ceram. Int. 43 (2017) 11469–11473, https://doi.org/10.1016/j.ceramint.2017.05.273.

[16] S.M. Rafiaei, A. Kim, M. Shokouhimehr, Effect of solvent on nanostructure and luminescence properties of combustion synthesized Eu^{3+} doped yttria, Nanosci. Nanotechnol. Lett. 6 (2014) 692–696, https://doi.org/10.1166/NNL.2014.1818.

[17] T. Igarashi, M. Ihara, T. Kusunoki, K. Ohno, T. Isobe, M. Senna, Relationship between optical properties and crystallinity of nanometer Y_2O_3:Eu phosphor, Appl. Phys. Lett. 76 (2000) 1549–1551, https://doi.org/10.1063/1.126092.

[18] M.J. Weber, Inorganic scintillators: today and tomorrow, J. Lumin. 100 (2002) 35–45, https://doi.org/10.1016/S0022-2313(02)00423-4.

[19] E. Cavalli, M. Bettinell, A. Belletti, A. Speghini, Optical spectra of yttrium phosphate and yttrium vanadate single crystals activated with Dy^{3+}, J. Alloys Compd. 341 (2002) 107–110, https://doi.org/10.1016/S0925-8388(02)00079-8.

[20] L.G.V. Uitert, R.C. Linares, R.R. Soden, A.A. Ballman, Role of f-orbital electron wave function mixing in the concentration Quenching of Eu^{3+}, J. Chem. Phys. 36 (1962) 702–705, https://doi.org/10.1063/1.1732595.

[21] Barbara A. Miura, Natália H. Ferreira, Pollyanna F. Oliveira, Emerson H. de Faria, Denise C. Tavares, Lucas A. Rocha, Katia J. Ciuffi, Eduardo J. Nassar, Functionalization of luminescent YVO_4:Eu^{3+} nanoparticles by sol–gel, J. Lumin. 159 (2015) 93–99, https://doi.org/10.1016/j.jlumin.2014.10.061.

[22] Seyed Mahdi Rafiaei, Mohammadreza Shokouhimehr, Impact of process parameters on luminescence properties and nanostructure of YVO_4: Eu phosphor, Mater. Chem. Phys. 229 (2019) 431–436, https://doi.org/10.1016/j.matchemphys.2019.03.046.

[23] Y.C. Chen, S.C. Huang, Y.K. Wang, Y.T. Liu, T.K. Wu, T.M. Chen, Ligand–functionalization of BPEI–coated YVO_4:Bi^{3+}, Eu^{3+} nanophosphors for tumor–cell–targeted imaging applications, Chem. Asian J. 8 (2013) 2652–2659, https://doi.org/10.1002/asia.201300570.

[24] L. Zhu, J.Y. Li, Q. Li, X.D. Liu, J. Meng, X.Q. Cao, Sonochemical synthesis and photoluminescent property of YVO_4:Eu nanocrystals, Nanotechnology 18 (2007) 55604–55609, https://doi.org/10.1088/0957-4484/18/5/055604.

[25] D. Hreniak, P. Doskocz, P. Guchowski, R. Lisiecki, W. Stręk, N. Vu, D.X. Loc, T. K. Anh, M. Bettinelli, A. Speghini, Enhancement of luminescence properties of $Eu^3$$^+$: YVO_4 in polymeric nanocomposites upon UV excitation, J. Lumin. 131 (2011) 473–476, https://doi.org/10.1016/j.jlumin.2010.10.028.

[26] M. Yoshimura, K. Byrappa, Hydrothermal processing of materials: past, present and future, J. Mater. Sci. 43 (2008) 2085–2103, https://doi.org/10.1007/s10853-007-1853-x.

[27] Huong Tran Thu, Vu Duc Tu, Tran Kim Anh, Vinh Le Thi, Minh Le Quoc, Fabrication and characterization of YVO_4:Eu^{3+} nanomaterials by the micro-wave technique, J. Rare Earths 29 (2011) 1137–1141, https://doi.org/10.1016/S1002-0721(10)60612-6.

[28] X.U. Shuilin, X.I.E. Xiaoji, Baozhou Zhao, N.I.E. Li, P.A.N. Yue, S.U. Haiquan, Ling Huang, Wei Huang, Synthesis and luminescent properties of lanthanide-doped $ScVO_4$ microcrystals, J. Rare Earths 35 (2017) 28–33, https://doi.org/10.1016/S1002-0721(16)60169-2.

[29] Tran Thu Huong, Le Thi Vinh, Thi Phuong Ha, Hoang Thi Khuyen, Tran Kim Anh, Vu Duc Tu, Le Quoc Minh, Controlled fabrication of the strong emission YVO_4:Eu^{3+} nanoparticles and nanowires by microwave assisted chemical synthesis, J. Lumin. 173 (2016) 89–93, https://doi.org/10.1016/j.jlumin.2016.01.003.

[30] E.V. Tomina, B.V. Sladkopevtsev, Mittova, V.O. Mittova, M.V. Knurova, A. N. Latyshev, I. Ya Mittova, Microwave synthesis and luminescence properties of YVO_4:Eu^{3+}, Inorg. Mater. 52 (2016) 495–498, https://doi.org/10.1134/S0020168516050174.

[31] Juan Wang, Mirabbos Hojamberdiev, Yunhua Xu, Jianhong Peng, Nonionic surfactant-assisted hydrothermal synthesis of YVO_4:Eu^{3+} powders in a wide pH range and their luminescent properties, Mater. Chem. Phys. 125 (2011) 82–86, https://doi.org/10.1016/j.matchemphys.2010.08.075.

[32] Liusai Yang, Guangshe Li, Minglei Zhao, Jing Zheng, Xiangfeng Guanb, Liping Li, Preparation and morphology-sensitive luminescence properties of Eu^{3+}-doped

YVO$_4$: a defect chemistry viewpoint of study, CrystEngComm 14 (2012) 3227–3235, https://doi.org/10.1039/C2CE06568A.

[33] S. Erdei, Preparation of YVO$_4$ powder from the Y$_2$O$_3$ + V$_2$O$_5$ + H$_2$O system by a hydrolysed colloid reaction (HCR) technique, J. Mater. Sci. 30 (1995) 4950–4959, https://doi.org/10.1007/BF01154509.

[34] H. Schwarz, Über die Chromate(V) der Seltenen Erden. IV Yttriumchromat(V), YCrO$_4$, Z. Anorg. Allg. Chem. 322 (1963) 137–143, https://doi.org/10.1002/zaac.19633220304.

[35] H.M. Rietveld, A profile refinement method for nuclear and magnetic structures, J. Appl. Crystallogr. 2 (1969) 65–71, https://doi.org/10.1107/S0021889869006558.

[36] J. Rodriguez-Carvajal, Recent advances in magnetic structure determination by neutron powder diffraction, Phys. B Condens. Matter 192 (1993) 55–69, https://doi.org/10.1016/0921-4526(93)90108-I.

[37] P. Debye Scherrer, Gottinger Nachrichten Gesell 2 (1918) 98.

[38] R.D. Shannon, Revised effective ionic radii and systematic studies of interatomic distances in halides and chalcogenides, Acta Crystallogr. A 32 (1976) 751–767, https://doi.org/10.1107/S0567739476001551.

[39] R. Jacob, J. Isac, X-ray diffraction line profile analysis of Ba$_{0.6}$Sr$_{0.4}$Fe$_x$Ti$_{(1-x)}$ O$_{3-\delta}$, (x=0.4), Int. J. Chem. Stud. 2 (5) (2015) 12–21.

[40] J. Mahapatro, S. Agrawal, Composition-dependent structural, physical, optical, and electrical properties of Ba$_{0.5}$Ca$_{0.5}$EuxFe$_{12-x}$O$_{19}$ hexaferrites for prospective applications, J. Mater. Sci. Mater. Electron. 34 (2023) 1838, https://doi.org/10.1007/s10854-023-111912.

[41] Jingyu Shao, Jinghui Yan, Xiaoguang Li, Shuang Li, Tao Hu, Novel fluorescent label based on YVO$_4$: Bi^{3+}, Eu^{3+} for latent fingerprint detection, J. Dyes a Pigm. 160 (2019) 555–562, https://doi.org/10.1016/j.dyepig.2018.08.033.

[42] A. Blachman, F. Funez, A.M. Birocco, S.L. Saavedra, J.M. Lázaro-Martinez, S. A. Camperi, R. Glisoni, A. Sosnik, G.C. Calabrese, Targeted anti-inflammatory peptide delivery in injured endothelial cells using dermatan sulfate/chitosan nanomaterials, Carbohydr, Polymers 230 (2020), 115610, https://doi.org/10.1016/j.carbpol.2019.115610.

[43] A.A. Kalinichev, M.A. Kurochkin, E.V. Golyeva, A.V. Kurochkin, E. Lähderanta, M. D. Mikhailov, I.E. Kolesnikov, Near-infrared emitting YVO$_4$:Nd^{3+} nanoparticles for high sensitive fluorescence thermometry, J. Lumin. 195 (2018) 61–66, https://doi.org/10.1016/j.jlumin.2017.11.024.

[44] I.E. Kolesnikov, A.A. Kalinichev, M.A. Kurochkin, D.V. Mamonova, E. Y. Kolesnikov, A.V. Kurochkin, et al., New strategy for thermal sensitivity enhancement of Nd^{3+}-based ratiometric luminescence thermometers, J. Lumin. 192 (2017) 40–46, https://doi.org/10.1016/j.jlumin.2017.06.024.

[45] M. Yu, J. Lin, J. Fu, Y.C. Han, Sol–gel fabrication, patterning and photoluminescent properties of LaPO$_4$:Ce^{3+}, Tb^{3+} nanocrystalline thin films, Chem. Phys. Lett. 371 (2003) 178–183, https://doi.org/10.1016/S0009-2614(03)00239-2.

[46] J.L. Zhang, J.X. Shi, J.B. Tan, X.J. Wang, M.L. Gong, Morphology-controllable synthesis of tetragonal LaVO$_4$ nanostructures, CrystEngComm 12 (2010) 1079–1085, https://doi.org/10.1039/B917526A.

[47] Yali Liu, Hailong Xiong, Nannan Zhang, Zhihua Leng, Ruiqing Li, Shucai Gan, Microwave synthesis and luminescent properties of YVO$_4$:Ln^{3+} (Ln = Eu, Dy and Sm) phosphors with different morphologies, J. Alloys Compd. 653 (2015) 126–134, https://doi.org/10.1016/j.jallcom.2015.09.015.

[48] D.L. Dexter, A theory of sensitized luminescence in solids, J. Chem. Phys. 21 (1953) 836–850, https://doi.org/10.1063/1.1699044.

[49] Th Forster, Zwischenmolekulare Energiewanderung und Fluoreszenz, Ann. Phys. 437 (1948) 55–75, https://doi.org/10.1002/andp.19484370105.

[50] B.M. Antipeuko, I.M. Bataev, V.L. Ermolaev, E.I. Lyubimov, T.A. Privalova, Radiationless transfer of electron excitation energy between rare-earth ions in POCl$_3$–SnCl$_4$, Opt. Spectrosc. 29 (1970) 335–338. http://inis.iaea.org/search/search.aspx?orig_q=RN:01003275.

[51] D.L. Dexter, J.A. Schulman, Theory of concentration quenching in inorganic phosphors, J. Chem. Phys. 22 (1954) 1063–1071, https://doi.org/10.1063/1.1740265.

[52] S. Shionoya, W.M. Yen, H. Yamamoto, Phosphor Handbook, second ed., CRC Press, Boca Raton, 2007, p. 1080, https://doi.org/10.1201/9781315222066.

[53] G. Blasse, Energy transfer in oxidic phosphors, Phys. Lett. 28 (1968) 444–445, https://doi.org/10.1016/0375-9601(68)90486-6.

[54] G. Mialon, S. Turkcan, A. Alexandrou, T. Gacoin, J.-P. Boilot, New insights into size effects in luminescent oxide nanocrystals, J. Phys. Chem. C 113 (2009) 18699–18706, https://doi.org/10.1021/JP907176X.

[55] J.L. Zhang, J.X. Shi, J.B. Tan, X.J. Wang, M.L. Gong, Morphology-controllable synthesis of tetragonal LaVO$_4$, CrystEngComm 12 (2010) 1079–1085, https://doi.org/10.1039/B917526A.

[56] Fei He, Piaoping Yang, Na Niu, Wenxin Wang, Shili Gai, Dong Wang, Jun Lin, Hydrothermal synthesis and luminescent properties of YVO$_4$:Ln^{3+} (Ln = Eu, Dy, and Sm) microspheres, J. Colloid Interface Sci. 343 (2010) 71–78, https://doi.org/10.1016/j.jcis.2009.11.025.

[57] T. Yan, D. Zhang, L. Shi, H. Yang, H. Mai, J. Fang, Refux synthesis, formation mechanism, and photoluminescence performance of monodisperse Y$_2$O$_3$:Eu^{3+} nanospheres, Mater. Chem. Phys. 117 (2009) 234–243, https://doi.org/10.1016/j.matchemphys.2009.05.047.

[58] K. Vini, H.P. Kumar, K.M. Nissamudeen, Red light emission of Y$_2$O$_3$:Eu^{3+} nanophosphors and luminescent enhancement by the addition of gadolinium oxide as co-dopant, J. Mater. Sci. Mater. Electron. 31 (2020) 5653–5666, https://doi.org/10.1007/s10854-020-03132-0.

[59] G. Blasse, Luminescence of inorganic solids: from isolated centres to concentrated systems, Prog. Solid State Chem. 18 (1988) 119, https://doi.org/10.1016/0079-6786(88)90004-0.

[60] Yuhua Wang, Yinyan Zuo, Hui Gao, Luminescence properties of nanocrystalline YVO$_4$:Eu^{3+} under UV and VUV excitation, Mater. Res. Bull. 41 (2006) 2147–2153, https://doi.org/10.1016/j.materresbull.2006.03.034.

[61] J. Wang, M. Hojamberdiev, Y. Xu, CTAB-assisted hydrothermal synthesis of YVO$_4$: Eu^{3+} powders in a wide pH range, Solid State Sci. 14 (2012) 191–196, https://doi.org/10.1016/j.solidstatesciences.2011.10.019.

[62] C. Li, Z. Hou, C. Zhang, P. Yang, G. Li, Z. Xu, Y. Fan, J. Lin, Controlled synthesis of Ln^{3+} (ln = Tb, Eu, Dy) and V^{5+} ion-doped YPO$_4$ nano-/microstructures with tunable luminescent colors, Chem. Mater. 21 (2009) 4598–4607, https://doi.org/10.1021/CM901658K.